A Hidden Markov Model for Seismocardiography

Johan Wahlström, Isaac Skog, *Member, IEEE*, Peter Händel, *Senior Member, IEEE*, Farzad Khosrow-khavar, *Member, IEEE*, Kouhyar Tavakolian, *Member, IEEE*, Phyllis K. Stein, and Arye Nehorai, *Fellow, IEEE*

***Abstract*—We propose a hidden Markov model approach for processing seismocardiograms. The seismocardiogram morphology is learned using the expectation-maximization algorithm, and the state of the heart at a given time instant is estimated by the Viterbi algorithm. From the obtained Viterbi sequence, it is then straightforward to estimate instantaneous heart rate, heart rate variability measures, and cardiac time intervals (the latter requiring a small number of manual annotations). As is shown in the conducted experimental study, the presented algorithm outperforms the state-of-the-art in seismocardiogram-based heart rate and heart rate variability estimation Moreover, the isovolumic contraction time and the left ventricular ejection time are estimated with mean absolute errors of about $5\,[ms]$ and $9\,[ms]$, respectively. The proposed algorithm 1) can be applied to any set of inertial sensors; 2) does not require access to any additional sensor modalities; 3) does not make any assumptions on the seismocardiogram morphology; and 4) explicitly models sensor noise and beat-to-beat variations (both in amplitude and temporal scaling) in the seismocardiogram morphology. As such, it is well-suited for low-cost implementations using off-the-shelf inertial sensors and targeting e.g., at-home medical services.**

***Index Terms*—Seismocardiogram, heart rate variability, cardiac time intervals, hidden Markov model.**

I. Introduction

Cardiovascular disease is the leading global cause of death, accounting for about 17 million deaths per year and with estimated annual costs of $320 billion [1]. The most commonly employed modality for assessing cardiac function is the electrocardiogram (ECG), which is a recording of the time-dependent voltage measured by electrodes placed on the body. In each cardiac cycle, the ECG demonstrates a distinctive waveform whose largest deflections can be found in the QRS complex. Often, the beat-to-beat interval is estimated as the time interval between two successive R peaks, the so called RR-interval. Later, we will also make use of the term NN-interval, referring to the RR-interval between two successive beats produced by sinus node depolarizations, i.e., excluding intervals affected by ectopic beats [2]. Although the ECG remains the standard diagnostic tool for cardiovascular disease, there is an increasing interest in alternative methods based on e.g., the photoplethysmogram (PPG) [3], the impedance cardiogram (ICG) [4], the phonocardiogram (PCG) [5], or the ballistocardiogram (BCG) [6]. In this study, our primary concern is the seismocardiogram (SCG)[1] [8]. Although SCGs traditionally have been recorded using accelerometers, recent studies have also employed gyroscopes [9], [10]. The vibrations can be studied along the superior-inferior axis (head-to-foot), the sinistro-dexter axis (left-to-right), and the dorsoventral axis (back-to-front). Most of the translational vibrations are concentrated along the dorsoventral axis, and hence, this has been considered the most important axis in accelerometer-based SCGs[2] [11]. SCGs offer several advantages over competing sensor modalities. These include the possibility of utilizing sensors embedded into personal devices such as smartphones (enabling a variety of at-home medical services) [12], the non-invasive nature of the method, and the low development cost of the sensors. The cost of a mass-produced inertial measurement unit (IMU), comprising three accelerometers and three gyroscopes, can be expected to be less than $1 [13]. To conclude, the SCG compares favorably to the ECG in terms of both availability and cost (but typically not in terms of accuracy), and can to some extent also be said to provide a different type of information (mechanical rather than electrical).

Normally, the data recorded from IMUs fixed to the sternum will reflect both respiratory motions and cardiac vibrations.

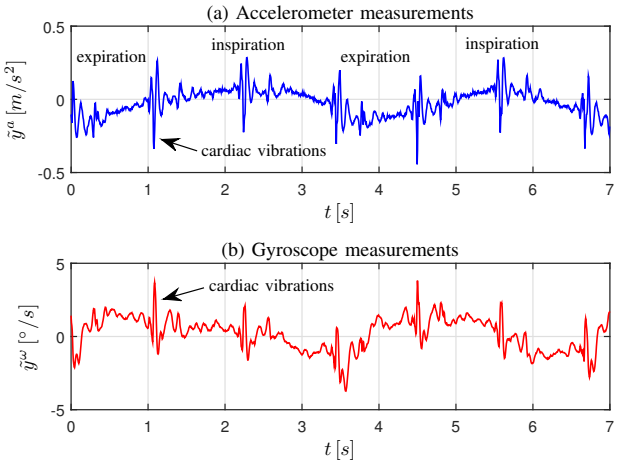

Fig. 1. Accelerometer and gyroscope measurements along the dorsoventral and sinistro-dexter axes, respectively.

J. Wahlström, I. Skog, and P. Händel are with the ACCESS Linnaeus Center, Dept. of Signal Processing, KTH Royal Institute of Technology, Stockholm, Sweden. (e-mail: {jwahlst, skog, ph}@kth.se).

F. Khosrow-khavar is with the MENRVA Research Group, School of Engineering Science at Simon Fraser University 8888 University Drive, Burnaby, BC, V5A 1S6, Canada (e-mail: fkhosrow@sfu.ca).

K. Tavakolian is with the Electrical Engineering Department, University of North Dakota, Room 160N, Upson II, 243 Centennial Drive, ND 58202 USA (e-mail: kouhyar@und.edu).

P. K. Stein is with the School of Medicine, Washington University in St. Louis, MO 63108 USA (e-mail: pstein@wustl.edu).

A. Nehorai is with the Preston M. Green Department of Electrical and Systems Engineering, Washington University in St. Louis, MO 63130 USA (e-mail: nehorai@ese.wustl.edu).

[1]While some studies use the terms BCG and SCG somewhat interchangeably, the general agreement is that the BCG represents recoil forces of the body to blood ejected by the heart, while the SCG represents local vibrations caused by the heart's contractions and relaxations [7].

[2]On the other hand, the data collected in this study indicates that the rotational vibrations are primarily concentrated along the superior-inferior and sinistro-dexter axes.

This is exemplified in Fig. 1, which shows accelerometer and gyroscope measurements along the dorsoventral and sinistro-dexter axes, respectively. The measurements were recorded over two respiratory cycles. As should be intuitive, the respiratory contribution in Fig. 1 (a) bears close resemblance to a sine wave. Moreover, each heartbeat in Fig. 1 can be seen to generate a characteristic wave pattern. While several attempts have been made to map different parts of this pattern to events in the cardiac cycle, this is still not a fully resolved issue [11], [14]. However, it should be noted that the characterizing features of the most important cardiac events in the SCG waveform (along the dorsoventral axis of the accelerometer measurements) has been widely agreed upon in the literature [15]. The morphology of the SCG signal is affected by several factors, including the sensor placement [11], the heart rate [12], the state of respiration [16], medical conditions of the subject [17], the age of the subject [18], and the occurrence of ectopic events [19]. Generally, SCGs will be more intricate and have more interpersonal variations than ECGs. As a result, heartbeat detectors adapted to ECGs tend to be perform poorly when applied to SCGs [20]. Next, we will discuss three potential capabilities of seismocardiograms, namely, heart rate estimation, the assessment of heart rate variability (HRV), and the estimation of cardiac time intervals.

A. Heart Rate Estimation

One method for estimating heart rate from SCGs is to detect each heartbeat individually as a sampling instance around which large signal deflections are concentrated. For this purpose, different combinations of band-pass filters, wavelet transforms, and envelope functions have been used [21], [22]. The shortcoming of these methods is that they detect heartbeats solely based on vibration peaks and their time points, while discarding any additional information provided by the recurrent vibration pattern.

An alternative method is to take sliding windows of the signal and transform them, one by one, to the frequency domain. The average heart rate over each window is then estimated as the frequency that maximizes the power spectral density (PSD) of the corresponding windowed signal. The window should include at least two heartbeats, with previously employed window lengths chosen in the interval $(20, 30)\,[s]$ [23], [24]. A similar method was used in [25], which attempted to find local maximums of the autocorrelation function of a windowed BCG. In [25], the window length was chosen as the smallest interval that was expected to fit at least two heartbeats. Unfortunately, these methods are only heuristically motivated, and it is not clear how their performance is affected when the vibrational pattern resulting from each heartbeat is stretched in time (events of this kind has previously been described in [14] and [26]).

B. Assessment of Heart Rate Variability

Variations in heart rate reflect complex interactions between the *parasympathetic* nervous system, which works to decrease the heart rate, and the *sympathetic* nervous system, which works to increase the heart rate. Even though the exact nature of these interactions remain the subject of active debate, measures of HRV have found use in a variety of clinical applications. For example, studies of HRV can be used for detecting increased mortality risks following a heart attack [27], for classifying sleep stages [28], and for assessing the risk of developing hypertension [29]. Common measures of HRV include time domain features such as standard deviations of the beat-to-beat interval, and frequency domain features such as ratios of spectral powers (of the beat-to-beat interval) at low and high frequencies [30]. Normally, a healthy heart exhibits a high HRV and utilizes a wide range of heart rates to cope with the stresses of daily life.

C. Time Interval Estimation

It is often of interest to estimate the time interval between two events in the cardiac cycle [31]. Cardiac time intervals have for example been used for the prognosis of patients recovering from myocardial infarction and for the detection of hypovolemia [32]. Many of the considered events can be identified from the SCG. These include the mitral valve closure (MC), the isovolumic moment (IM), the aortic valve opening (AO), and the aortic valve closure (AC)[3] [15]. Typically, these events are detected as sampling instances where the accelerometer signal along the dorsoventral axis attains local maximums or minimums. Often, the data is preprocessed using a combination of band-pass filters, wavelet transforms, and envelope functions [15], [20], [33]–[36]. Commonly studied time intervals which can be estimated using only cardiac events detected from the SCG include the isovolumic contraction time (IVCT), defined as the time from the MC to the AO, and the left ventricular ejection time (LVET), defined as the time from the AO to the AC. Most methods for the identification of cardiac events from an SCG first detect fiducial points from an ECG and then make assumptions on the temporal distance between these fiducial points and specific cardiac events.

D. Contributions

We propose a hidden Markov model (HMM) approach to SCGs. The idea is to divide the cardiac vibration into a set of hidden states, which only are allowed to be traversed in a sequential manner. This enables the estimation of instantaneous heart rate, HRV indices, and cardiac time intervals, using information from the full waveform of cardiac vibrations. Performance evaluations are carried out using data from 67 subjects. The proposed method is shown to outperform the current state-of-the-art among envelope and spectral-based methods for heart rate estimation, while providing highly accurate estimates of standard HRV measures and cardiac time intervals.

Reproducible research: The data used in this paper is available at www.kth.se/profile/jwahlst/ together with a Matlab implementation of the proposed method.

[3]The set of cardiac events that can be detected will depend on the considered modality. For example, the ECG cannot be used to detect the AO.

II. Model and estimation framework

The heartbeat vibrations are described using a HMM. Since the HMM depends on a number of unknown parameters, we learn these parameters using the Baum-Welch algorithm. Following this, the most likely sequence of states is found by the Viterbi algorithm. Last, we estimate the time point of each individual heartbeat. While similar models have been proposed for ECGs, these have typically relied on manual annotations during the training phase [37], [38], and the associated publications have seldom presented any performance characterizations of beat-to-beat interval estimates.

A. State-space Model

Consider a stochastic process $\{x_k\}_{k=0}^K$. At each sampling instance k, the variable x_k is in one of the "hidden" states $\{1, 2, \dots, N+1\}$. Here, we make the interpretation

$$\textit{State } 1\text{: No vibration due to heartbeats.} \tag{1a}$$

and for $n > 0$

$$\textit{State } n+1\text{: The } n\text{th step in the wave pattern of vibrations due to a heartbeat.} \tag{1b}$$

Formulated in words, the wave pattern seen in the inertial measurements during a heartbeat is divided into N states. In addition, we use a dummy state to capture noise in between the vibrations caused by two heartbeats. For short, we shall write $x_k = n$ as $x_k^{(n)}$ for any k and n.

The probabilities of different state transitions are given by $A_{nm} \triangleq p(x_{k+1}^{(m)} | x_k^{(n)})$, where $p(\cdot|\cdot)$ denotes a conditional probability mass function (pmf). In every cardiac cycle, the Markov chain is expected to traverse each of the $N+1$ states in a sequential manner. Therefore, it is assumed that the HMM is cyclic, so that $A_{nm} = 0$ for all n and m except $n = m$, $n+1 = m$, and $[n\ m] = [N+1\ 1]$. By letting A_{nn} be nonzero for $n > 1$, we allow for some variability in the time length of different subpatterns in the SCG waveform.

To separate the cardiac vibrations from the respiratory motion, we first subtract the mean from each accelerometer and gyroscope signal, and then high-pass filter the signals using a Butterworth filter of order three and with a cutoff frequency of $2\,[Hz]$. This will not only remove the larger part of the respiratory contribution, but also part of the cardiac signal (some spectral overlap is typically present [39]). The practice of high-pass filtering the raw SCG signal has been well established in the literature [21]–[23]. The high-pass filtered inertial measurements are used as input in the HMM, and are modeled as

$$\mathbf{y}_k = \mathbf{h}\big(x_k^{(n)}\big) + \boldsymbol{\epsilon}_k. \tag{2}$$

Here, we could have $\mathbf{y}_k \triangleq [(\mathbf{y}_k^a)^\intercal\ (\mathbf{y}_k^\omega)^\intercal]^\intercal$, where $\mathbf{y}_k$ includes both three-dimensional accelerometer measurements $\mathbf{y}_k^a$ and three-dimensional gyroscope measurements $\mathbf{y}_k^\omega$. However, the presented framework can easily be modified to only use a subset of these measurements, e.g., only accelerometer measurements along the dorsoventral axis. For notational convenience, we define $\boldsymbol{\mu}_n \triangleq \mathbf{h}(x_k^{(n)})$.

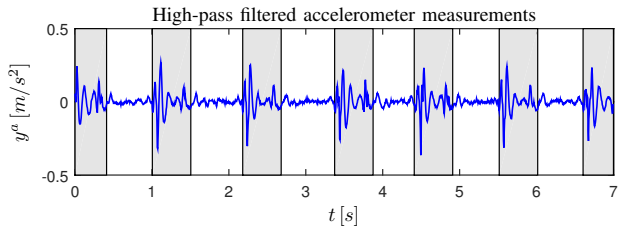

Fig. 2. High-pass filtered accelerometer measurements along the dorsoventral axis. The measurements within the shaded areas are used to initialize $\hat{\boldsymbol{\mu}}_n$.

The measurement noise $\boldsymbol{\epsilon}_k$ is assumed to be normally distributed and white. If the measurements are taken from a 6-degrees of freedom IMU, the covariance becomes

$$\mathbf{R} \triangleq \begin{bmatrix} \sigma_a^2 \mathbf{I}_3 & \mathbf{0}_3 \\ \mathbf{0}_3 & \sigma_\omega^2 \mathbf{I}_3 \end{bmatrix} \tag{3}$$

where the parameters σ_a and σ_ω need to take both sensor noise and variations in the SCG morphology into account. Here, $\mathbf{0}_\ell$ and $\mathbf{I}_\ell$ denote $\ell \times \ell$-dimensional zero and identity matrices, respectively.

B. Baum-Welch Algorithm

The expectation-maximization (EM) algorithm is an iterative method for estimating the parameters of a statistical model that depends on some hidden states. When applied to HMMs, the algorithm is known as the Baum-Welch algorithm [40]. We use the Baum-Welch algorithm to find an approximation to the maximum likelihood (ML) estimate

$$\hat{\lambda} = \arg\max_{\lambda} p(\mathbf{y}_0, \dots, \mathbf{y}_L | \lambda). \tag{4}$$

Here, $\lambda \triangleq \{\{\pi_n\}, \{A_{nm}\}, \{\boldsymbol{\mu}_n\}\}$ collects the model parameters, $\pi_n \triangleq p(x_0^{(n)})$ is the initial state probability, and $p(\cdot|\cdot)$ denotes a conditional probability density function (pdf). For computational reasons, the Baum-Welch algorithm is only applied to a subset $\{\mathbf{y}_k\}_{k=0}^L$ of the total set of available measurements $\{\mathbf{y}_k\}_{k=0}^K$. Note that the measurement covariance matrix $\mathbf{R}$ is excluded from λ since both σ_a and σ_ω are considered to be known.

Assuming that the sequential parameter estimates are $\{\hat{\lambda}^{(1)}, \hat{\lambda}^{(2)}, \dots\}$, the parameter estimates are updated until

$$\frac{\log p(\mathbf{y}_0, \dots, \mathbf{y}_L | \hat{\lambda}^{(i+1)}) - \log p(\mathbf{y}_0, \dots, \mathbf{y}_L | \hat{\lambda}^{(i)})}{\log p(\mathbf{y}_0, \dots, \mathbf{y}_L | \hat{\lambda}^{(i)})} < \eta \tag{5}$$

where $\log(\cdot)$ denotes the natural logarithm. For further details on the Baum-Welch algorithm, refer to [41] and references therein.

C. Initialization of the Baum-Welch Algorithm

As noted in [41], there is usually no obvious way of initializing the Baum-Welch recursions. In this paper, we set

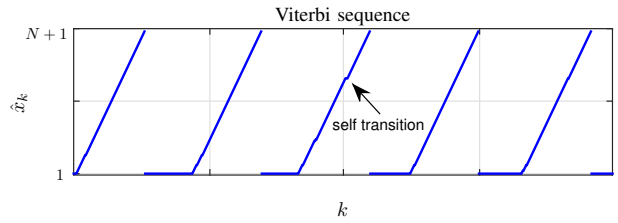

Fig. 3. Example of a Viterbi sequence $\{\hat{x}_k\}$ over five detected heartbeats.

$\hat{\pi}_n^{(0)} = 1/(N+1)$ for all n, as well as

$$\hat{A}_{nm}^{(0)} = \begin{cases} 0.98, & n = 1,\ m = 1 \\ 0.02, & n = 2,\dots,N+1,\ m = n \\ 0.02, & n = 1,\ m = 2 \\ 0.98, & n = 2,\dots,N,\ m = n+1 \\ 0.98, & n = N+1,\ m = 1. \end{cases} \tag{6}$$

To initialize $\hat{\boldsymbol{\mu}}_n$, we attempt to find intervals of length N over which the signal energy is locally maximized. The initialization is then made based on the signal values within these intervals. Hence, assuming that the measurements are taken from a 6-degrees of freedom IMU, we begin by computing the normalized energy function

$$E_k = \frac{\sum_{\ell_1=k}^{k+N-1} \|\mathbf{y}_{\ell_1}^{\omega}\|^2}{\sum_{k_1=0}^{L+N-1} \|\mathbf{y}_{k_1}^{\omega}\|^2} + \frac{\sum_{\ell_2=k}^{k+N-1} \|\mathbf{y}_{\ell_2}^{a}\|^2}{\sum_{k_2=0}^{L+N-1} \|\mathbf{y}_{k_2}^{a}\|^2} \tag{7}$$

where $\|\cdot\|$ denotes the Euclidean norm. Following this, we identify all sampling instances where $E_k = \max(E_{k-\delta k},\dots,E_{k+\delta k},)$. These sampling instances are denoted $\{j_1, j_2, \dots, j_J\}$. Here, δk is some chosen positive integer. Normally, $\{(j_1, j_1+N-1), (j_2, j_2+N-1), \dots, (j_J, j_J+N-1)\}$ will be sets of samples over which similar cardiac vibrations have been recorded. This is illustrated in Fig. 2 which shows high-pass filtered accelerometer measurements along the dorsoventral axis, with the aforementioned intervals shaded in grey. The measurements are taken from the same time interval as in Fig. 1. Finally, $\hat{\boldsymbol{\mu}}_n$ is initialized as $\hat{\boldsymbol{\mu}}_1^{(0)} = \mathbf{0}_{3,1}$ and

$$\hat{\boldsymbol{\mu}}_n^{(0)} = \frac{1}{J}\sum_{l=1}^{J} \mathbf{y}_{j_l+n-2} \tag{8}$$

for $n = 2,\dots,N+1$. Here, $\mathbf{0}_{\ell_1,\ell_2}$ denotes the zero matrix of dimension $\ell_1 \times \ell_2$.

Even if the specified HMM would have been the true underlying model of the studied data, the Baum-Welch algorithm would not have been guaranteed to converge to the globally optimal solution, i.e., the maximum likelihood estimate [42]. However, the specified initialization always resulted in parameter estimates that agreed with basic intuition.

D. Viterbi Algorithm

Now, assume that the Baum-Welch algorithm has converged and that the final estimate is $\hat{\lambda}$. We then use the Viterbi algorithm [41] to find the maximum a posteriori (MAP) estimate

$$\{\hat{x}_k\} \triangleq \arg\max_{x_0,\dots,x_K} p(x_0,\dots,x_K|\mathbf{y}_0,\dots,\mathbf{y}_K,\hat{\lambda}) \tag{9}$$

of the complete sequence of states $\{x_k\}_{k=0}^K$. Note that Viterbi sequence always is valid in the sense that $p(\hat{x}_0,\dots,\hat{x}_K|\mathbf{y}_0,\dots,\mathbf{y}_K,\hat{\lambda}) > 0$ (all its state transitions will be permissible). Hence, the sequence $\{\hat{x}_k\}_{k=0}^K$ is guaranteed to unambiguously indicate when a heartbeat is considered to have been detected. A typical Viterbi sequence over five heartbeats is illustrated in Fig. 3. As indicated in Fig. 3, the number of self-transitions $\{\hat{x}_k^{(n)}, \hat{x}_{k+1}^{(n)}\}$ for $n > 1$ over a single heartbeat is usually small in comparison to N.

Algorithm 1 : Heartbeat detection.

```
Set i = 0 and k = min {k' : x̂_{k'} = 1}
while N + 1 ∈ {x̂_k, ..., x̂_K} do
    l := k
    if x̂_k > 1 then
        if x̂_k = 2 then
            i := i + 1
        end if
        while x̂_{l+1} = x̂_k do
            l := l + 1
        end while
        t_i^{(x̂_k)} = (k + l)/(2 f_s)
    end if
    k := l + 1
end while
```

E. Heart Rate Estimation

When the Viterbi sequence $\{\hat{x}_k\}_{k=0}^K$ has been identified, we can go on to estimate the beat-to-beat interval. Intuitively, the beat-to-beat interval is equal to the horizontal distance between two adjacent tilted stripes in Fig. 3. Based on this observation, we first compute the average time point $t_i^{(n)}$ at which $\{\hat{x}_k\}$ is in state n during the ith cardiac cycle (only states $n > 1$ are considered). The computations are shown in Algorithm 1, where f_s denotes the sampling rate. Since the nominal beat-to-beat interval $t_{i+1}^{(n)} - t_i^{(n)}$ may differ depending on which state n that is considered, the final estimates of the beat-to-beat intervals are computed by averaging over all states $n = 2,\dots,N+1$. Hence, the estimated beat-to-beat interval and instantaneous heart rate as implied by heartbeats i and $i+1$ are

$$\delta t_i \triangleq t_{i+1} - t_i \tag{10a}$$

and

$$\mathrm{HR}_i \triangleq \frac{1}{t_{i+1} - t_i}, \tag{10b}$$

respectively, where the estimated time point of heartbeat i is

$$t_i \triangleq \frac{1}{N}\sum_{n=2}^{N+1} t_i^{(n)}. \tag{11}$$

The sequences $\{\delta t_i\}$ and $\{\mathrm{HR}_i\}$ can then be used to obtain estimates of standard HRV indices [2].

Algorithm 2 : Summary of data inference.

1: *High-pass filtering*: Subtract the mean from each IMU signal, and then high-pass filter the signals using a Butterworth filter of order 3 and with a cutoff frequency of $2\,[Hz]$. The resulting signal is $\{\mathbf{y}_k\}_{k=0}^{K}$.

2: *Baum-Welch algorithm*: Approximate the ML estimate

$$\hat{\lambda} = \arg\max_{\lambda} p(\mathbf{y}_0, \ldots, \mathbf{y}_L|\lambda)$$

of the model parameters λ by employing the following two steps:

a) Compute the initial parameter estimate $\hat{\lambda}^{(0)}$ as described in Section II-C.

b) Update the parameter estimate using the Baum-Welch algorithm until (5) is satisfied.

3: *Viterbi algorithm*: Find the MAP estimate

$$\{\hat{x}_k\} \triangleq \arg\max_{x_0,\ldots,x_K} p(x_0, \ldots, x_K|\mathbf{y}_0, \ldots, \mathbf{y}_K, \hat{\lambda})$$

of the complete sequence of states $\{x_k\}_{k=0}^{K}$ by using the Viterbi algorithm.

4: *Heart rate and cardiac time interval estimation*: Estimate the time point $t_i^{(n)}$ of state n during heartbeat i as outlined in Algorithm 1. Finally, (10) and (11) give the estimated beat-to-beat interval and instantaneous heart rate, and (12) gives the estimated cardiac time intervals.

F. Time Interval Estimation

The estimation of cardiac time intervals can be performed in a manner analogous to that of the heart rate estimation. However, we first need to identify which states in the HMM that represent the events of interest. Here, we will assume that this is done by visual inspection of the estimated SCG waveform $\hat{\boldsymbol{\mu}}_n$. As a practical example, an experienced annotation expert may decide that the MC can be expected to occur at state 37. Hence, each cardiac event requires one manual annotation per subject. The cardiac time interval that describes the time passed between the events e and e' after the ith heartbeat can then be estimated as

$$\delta t_i^{EE'} = t_i^{(E')} - t_i^{(E)} \tag{12a}$$

if $E' > E$, or as

$$\delta t_i^{EE'} = t_{i+1}^{(E')} - t_i^{(E)} \tag{12b}$$

if $E' < E$. Here, E and E' are the states in the HMM that have been found to represent e and e', respectively, while $t_i^{(n)}$ is obtained as in Algorithm 1. Since the first state in the HMM is interpreted as a dummy state representing all sampling instances where no distinct vibrations occur, we will in practice assume that $E \neq 1$ and $E' \neq 1$. The full procedure of going from raw IMU measurements to heart rate or time interval estimates is summarized in Algorithm 2.

III. Experimental study

We begin this section by describing the two employed data sets. Then, the design parameters are presented, and the SCG morphology measured by a 6-degrees of freedom IMU is illustrated. Finally, we present the results of the estimation of heart rate, HRV measures, and cardiac time intervals.

TABLE I
DESCRIPTION OF DATA SETS.

Descriptor	Data set 1	Data set 2
# of subjects	1	66
Data/subject	$5\,[h]$	$1\,[min]$
Sampling rate (SCG)	$500\,[Hz]$	$500\,[Hz]$
Sampling rate (ECG)	$128\,[Hz]$	$2000\,[Hz]$
Manually annotated	No	Yes
SCG sensors	6-deg. IMU	one-axis acc.

TABLE II
DESIGN PARAMETERS.

Parameter	Value
σ_a	$0.1\,[m/s^2]$
σ_ω	$0.5\,[^\circ/s]$
L	10 000
η	10^{-2}
δk	150

A. Data Sets

Table I describes the studied data sets. All data was recorded with the subject in supine position. The first data set was recorded from an inertial array with 32 InvenSense MPU-9150 IMUs, placed about five centimeters to the left (as seen from the subject) of the lower sternum midpoint [43]. Details about the sensor array can be found in [44]. By averaging the data over the IMUs, the array was made to function as a single high-sensitive 6-degrees of freedom IMU. ECG data was recorded from a myPatch 3 Holter monitor. The subject was a healthy male, aged 26 years. The second data set consists of accelerometer measurements along the dorsoventral axis from 66 subjects. For further details on this data set, refer to the description of the SFU_GYM study in [15]. The R peaks in the ECG data were detected using the Pan-Tompkins algorithm [45], and the resulting beat-to-beat intervals were used as ground truth in Sections III-C and III-D.

The benefit of the first data set is that it can be used to compute a large number of realizations of standard HRV measures, while complying with the standard convention of computing the measures using NN-intervals obtained from five-minute data segments [2]. In addition, data from a 6-degrees of freedom IMU allows us to study both translational and rotational SCG morphology in all spatial directions. On the other hand, the second data set makes it possible to evaluate the presented algorithm on a diverse set of subjects with differing SCG characteristics. Moreover, it also includes manual annotations of the MC, IM, AO, and AC over all recorded data, which were used as ground truth in the evaluation of the cardiac time interval estimates in Section III-E. Since the manual annotations used in the training phase described in Section II-F were made based on parameter

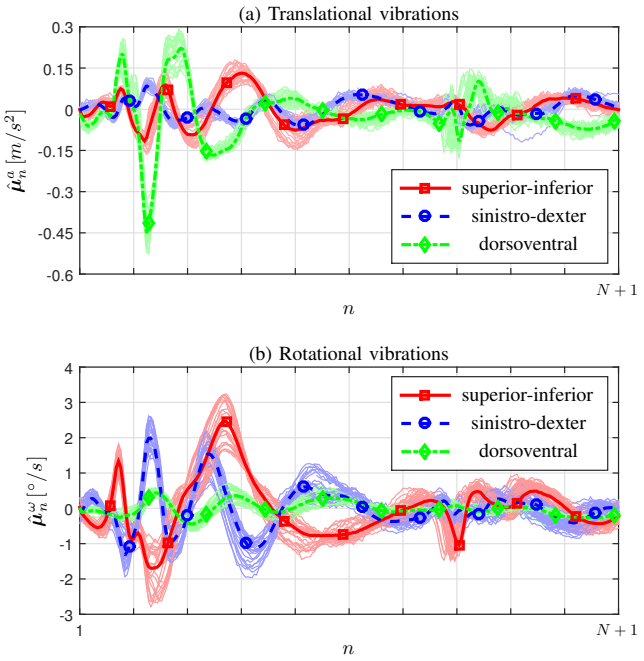

Fig. 4. Example of estimated and measured SCG morphology using (a) accelerometers and (b) gyroscopes.

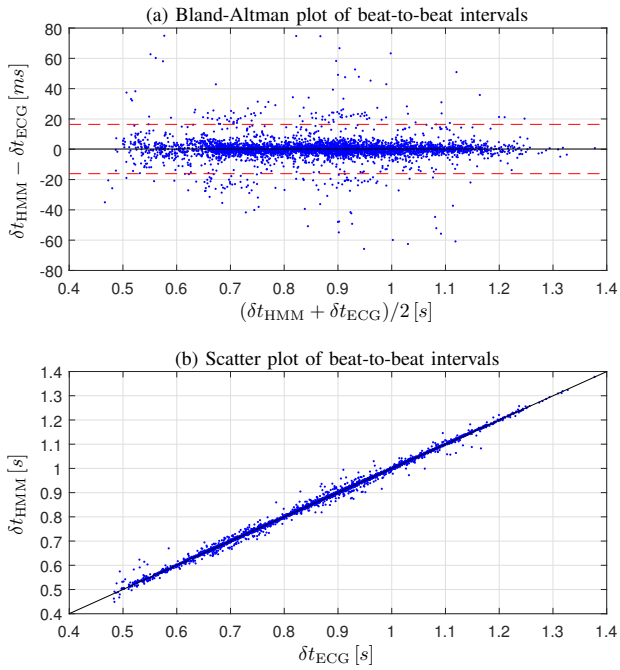

Fig. 5. Bland-Altman and scatter plot for the HMM with average error (the solid black line in the Bland-Altman plot), 95 [%]-limits of agreement (the dashed red lines in the Bland-Altman plot), and fitted linear regression line (the solid black line in the scatter plot). The sample correlation coefficient of δt_{HMM} and δt_{ECG} was 0.999.

estimates $\hat{\boldsymbol{\mu}}_n$ obtained from the first $L/f_s = 20\,[s]$ of data from each subject, the accuracy of the cardiac time interval estimates was evaluated on the remaining $40\,[s]$ of data.

B. Design Parameters and the SCG Morphology

The employed design parameters are detailed in Table II. Further, the number of states was chosen as $N = \lfloor 0.6 f_s/\overline{\mathrm{HR}}_S \rfloor$, where $\lfloor \cdot \rfloor$ denotes the floor function and $\overline{\mathrm{HR}}_S$ is the average heart rate as estimated by the spectral-based method presented in Appendix B. This means that the Markov process will be in the first state approximately $40\,[\%]$ of the time. Since the Viterbi sequence is expected to pass through each of the $N+1$ states during each individual cardiac cycle, there will always exist an upper bound, inversely proportional to N, on the estimated heart rate. However, a too small N will increase the risk of overestimating the heart rate.

Fig. 4 illustrates the SCG morphology in a randomly chosen segment in data set 1. For clarity, the translational vibrations, measured by the accelerometers, and the rotational vibrations, measured by the gyroscopes, are displayed separately. The estimated parameters $\hat{\boldsymbol{\mu}}_n^a$ and $\hat{\boldsymbol{\mu}}_n^\omega$ are displayed in thick lines. Here, $\hat{\boldsymbol{\mu}}_n = [(\hat{\boldsymbol{\mu}}_n^a)^\intercal \ (\hat{\boldsymbol{\mu}}_n^\omega)^\intercal]^\intercal$. Further, Fig. 4 also shows the corresponding measurements from 50 heartbeats in thin lines. In doing this, the state at a given sampling instance was estimated using the Viterbi algorithm. None of the displayed measurements were used in the estimation of $\boldsymbol{\mu}_n$.

C. Heart Rate Estimation

The HMM-based method for heart rate estimation presented in Section II was evaluated on both data sets. To benchmark its performance, we also applied previously proposed envelope and spectral-based methods, described in Appendix A and Appendix B, respectively, to the same data sets. Data from the first data set was processed in five-minute segments. In the second data set, data from each individual subject was processed independently.

Table III displays error measures of the estimated instantaneous heart rate HR and beat-to-beat interval δt for both data sets. The errors are quantified in terms of their mean absolute error (MAE) and normalized MAE (nMAE), i.e., the MAE divided by the time-averaged ECG-derived value of the variable. In addition, standard deviations of the absolute errors, with or without normalization, are added to characterize the error distributions. As can be seen from Table III, the HMM yields a substantial performance gain over previously proposed methods. Although the performance seems to be better on the first data set than on the second, it should be noted that this primarily is due to a small number of individuals in the second data set who had irregular SCG waveforms or other anomalies. To exemplify this, we mention that for 41 of the 66 subjects in second data set, the HMM resulted in a MAE of the beat-to-beat interval that was lower than the corresponding MAE obtained on the first data set ($4.28\,[ms]$). However, one should also take into account the comparatively low sampling rate of the ECG in the first data set. Since the detected R peaks always are chosen among the existing samples, the timing of an individual detected peak could have an absolute error up to $3.9\,[ms]$ on the first data set (the sampling rate was $128\,[Hz]$), even when assuming that the chosen sample is the one that is closest to the true peak. This uncertainty has most likely increased the apparent MAEs of the HMM on the first data set.

To further characterize the beat-to-beat intervals errors we display Bland-Altman and scatter plots for the HMM applied

TABLE III
ERRORS OF ESTIMATED BEAT-TO-BEAT INTERVAL AND HEART RATE.

	Data set 1			Data set 2		
	HMM	Envelope-based method	Spectral-based method	HMM	Envelope-based method	Spectral-based method
Absolute errors (mean ± standard deviation)						
HR $[bpm]$	0.29 ± 0.36	1.05 ± 2.68	4.55 ± 5.05	0.56 ± 2.74	5.00 ± 10.69	7.06 ± 10.61
$\delta t\,[ms]$	4.28 ± 6.52	16.64 ± 33.96	75.06 ± 76.29	6.10 ± 31.89	67.30 ± 146.86	82.17 ± 110.23
Normalized absolute errors (mean ± standard deviation)						
HR [%]	0.46 ± 0.59	1.69 ± 4.32	7.32 ± 8.13	0.78 ± 3.76	6.86 ± 14.66	9.69 ± 14.56
δt [%]	0.44 ± 0.66	1.69 ± 3.45	7.63 ± 7.75	0.71 ± 3.70	7.82 ± 17.07	9.55 ± 12.81

TABLE IV
ERRORS OF ESTIMATED HRV MEASURES.

	Data set 1			Data set 2		
	HMM	Envelope-based method	Spectral-based method	HMM	Envelope-based method	Spectral-based method
Absolute errors (mean ± standard deviation)						
SDNN $[ms]$	0.56 ± 0.27	8.90 ± 11.54	57.98 ± 22.75	11.40 ± 28.54	79.48 ± 75.88	67.90 ± 53.72
RMSSD $[ms]$	2.51 ± 2.81	20.89 ± 22.91	107.31 ± 35.41	16.25 ± 37.62	136.76 ± 123.93	115.13 ± 83.11
pNN50 [%]	0.89 ± 0.60	5.17 ± 5.31	20.71 ± 5.57	1.78 ± 1.99	135.92 ± 130.80	175.43 ± 10.21
VLF $\cdot 10^{-3}[(ms)^2]$	0.01 ± 0.04	0.04 ± 0.06	1.38 ± 1.21	0.11 ± 0.34	1.41 ± 2.93	1.16 ± 2.32
LF $\cdot 10^{-3}[(ms)^2]$	0.03 ± 0.05	0.14 ± 0.22	1.91 ± 1.65	0.60 ± 2.55	3.71 ± 6.71	2.63 ± 3.33
HF $\cdot 10^{-3}[(ms)^2]$	0.10 ± 0.09	1.13 ± 1.37	8.67 ± 4.52	1.27 ± 3.80	14.64 ± 18.51	9.75 ± 10.68
LF/HF	0.19 ± 0.28	0.28 ± 0.24	0.93 ± 0.63	0.57 ± 2.38	1.20 ± 3.19	1.20 ± 3.09
Normalized absolute errors (mean ± standard deviation)						
SDNN [%]	0.71 ± 0.34	11.23 ± 14.56	73.18 ± 28.72	17.32 ± 43.38	120.84 ± 115.37	103.23 ± 81.67
RMSSD [%]	3.51 ± 3.92	29.19 ± 32.01	149.95 ± 49.48	24.34 ± 56.34	204.83 ± 185.61	172.42 ± 124.47
pNN50 [%]	4.65 ± 3.14	27.11 ± 27.82	108.60 ± 29.20	14.37 ± 16.03	109.52 ± 105.40	141.36 ± 82.30
VLF [%]	0.47 ± 2.02	1.68 ± 2.83	62.94 ± 55.05	21.61 ± 64.64	272.03 ± 564.64	223.92 ± 447.18
LF [%]	1.41 ± 2.78	7.52 ± 11.72	103.43 ± 89.48	32.11 ± 137.76	199.80 ± 361.75	141.63 ± 179.40
HF [%]	5.12 ± 4.83	58.02 ± 70.66	445.83 ± 233.27	52.00 ± 155.02	597.80 ± 756.00	398.30 ± 435.99
LF/HF [%]	15.32 ± 22.43	21.82 ± 18.93	73.11 ± 49.33	34.96 ± 146.84	74.04 ± 197.02	74.13 ± 190.69

The variables were estimated using five minutes (data set 1) or one minute (data set 2) of data.

to the second data set in Fig. 5. Throughout the paper, we compute the 95 [%]-limits of agreement in the Bland-Altman plots by assuming normally distributed errors [46], and fit the regression lines in the scatter plots using a Huber loss function. The limits of agreement were $\pm 16\,[ms]$, which is somewhat better than the corresponding figures of $\pm 20\,[ms]$ reported in [47]. In accordance with [47], Fig. 5 and associated measures did not consider any absolute beat-to-beat interval errors that were larger than $100\,[ms]$ (these were considered to be false positives or missed beats). To illustrate the heavy-tailed nature of the beat-to-beat interval errors we visualize the empirical distribution functions (edfs) of the absolute heart rate errors, collected from both data sets, in Fig. 6.

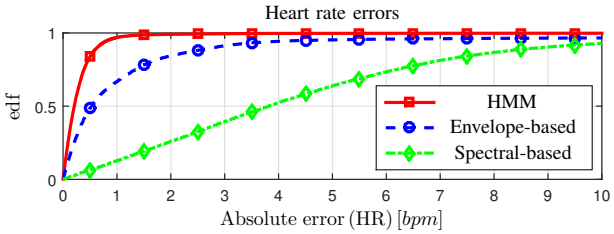

Fig. 6. Empirical distribution functions of the heart rate errors.

It is encouraging to compare the accuracy of the HMM with results reported in studies using BCG signals. For example, the beat-to-beat interval has previously been estimated with nMAEs in the intervals $(0.47, 1.06)\,[\%]$ [6] (8 subjects; sampling rate: $200\,[Hz]$) and $(0.49, 3.64)\,[\%]$ [48] (1 subject; sampling rate: $200\,[Hz]$), while another study reported a MAE of $14.16\,[ms]$ [49] (17 subjects; sampling rate: $128\,[Hz]$). Based on previous studies, the HMM also performed well in comparison to PPGs. For example, in [50], the PPG-based estimates of the beat-to-beat interval had a MAE of $6.68\,[ms]$. The study in [50] excluded false alarms and missed detections, and was conducted on 10 subjects with a sampling rate of $1\,[kHz]$). None of the studies reported any documented cardiac abnormality among the subjects.

Due to disparities in data quality and the absence of established reporting standards, is often difficult to compare the accuracies reported in different SCG studies. Many studies will for example exclude estimates with too large errors when computing error measures [21], [47], while others only report errors of time-averaged heart rates [9], [10], [23].

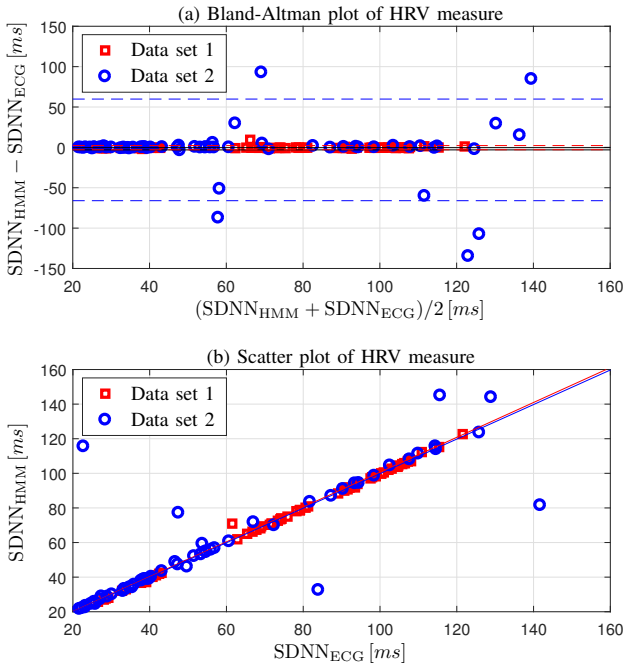

Fig. 7. Bland-Altman and scatter plot for the HMM with average errors (the solid black lines in the Bland-Altman plot), 95 [%]-limits of agreement (the dashed red and blue lines in the Bland-Altman plot for the first and second data set, respectively), and fitted linear regression lines (the solid red and blue lines in the scatter plot for the first and second data set, respectively). The sample correlation coefficient of $\mathrm{SDNN_{HMM}}$ and $\mathrm{SDNN_{ECG}}$ was 0.999 and 0.657 for estimates using the first and second data set, respectively.

D. HRV Measures

Standard HRV measures were estimated from both data sets. The studied HRV measures included the standard deviation of all NN-intervals (SDNN), the root-mean-squared differences of successive NN intervals (RMSSD), the ratio of the number of successive NN-intervals differing by more than $50\,[ms]$ to the total number of NN-intervals (pNN50), the PSD of the NN-sequence integrated over the very low frequency range $(0.003, 0.04)\,[Hz]$ (VLF), over the low frequency range $(0.04, 0.15)\,[Hz]$ (LF), over the high frequency range $(0.15, 0.4)\,[Hz]$ (HF), and the ratio of LF and HF (LF/HF) [2]. Since the NN-series are sampled unevenly in time (once per heartbeat), they were, for the computations of the spectral measures, resampled to a frequency of $1\,[Hz]$ using cubic splines [51].

The MAEs and the nMAEs of the considered HRV indices are presented in Table IV. As could have been expected from the preceding subsection, the HMM outperforms both the envelope and the spectral-based method on all accounts. The accuracy of the estimates is comparable to that of previous PPG-based estimates in [3], where the reported nMAEs of SDNN, RMSSD, VLF, LF, HF, and LF/HF were $14\,[\%]$, $16\,[\%]$, $39\,[\%]$, $18\,[\%]$, $27\,[\%]$, and $30\,[\%]$, respectively. The study in [3] was conducted on 4 subjects, acquired PPG data at a sampling rate of $21.33\,[Hz]$, and used polynomial interpolation to increase the precision of the detected heartbeats. Bland-Altman and scatter plots of the SDNN measure estimated using the HMM are shown in Fig. 7. As can be seen, the estimates are highly accurate for the great majority of the studied subjects. The clinical applicability of SCG-based HRV estimates will be highly dependent on the extent to which the reliability of individual estimates can be assessed, a topic which will need to be addressed in future studies

E. Cardiac Time Intervals

Table V shows the MAEs of the estimated time points for the four cardiac events MC, IM, AO, and AC, and of the estimated time intervals IVCT and LVET[4]. Fig. 8 displays Bland-Altman and scatter plots for the HMM estimates and the ground truth of the LVET. The estimates were obtained by applying the method described in Section II-F to the second data set. As can be seen, the MAE of the time points for the cardiac events is in the order of $5\,[ms]$. This can be compared to MAEs of the IM, AO, and AC at $9\,[ms]$, $9\,[ms]$, and $6\,[ms]$, respectively, for a previously presented SCG-based method conducted on 18 subjects with a sampling rate of $1\,[kHz]$ [52], and MAEs of the MC, AO, and AC at $12\,[ms]$, $17\,[ms]$, and $9\,[ms]$, respectively, for a PCG-based method conducted on 60 subjects, (51 of which suffered from congestive heart failure) with a sampling rate of $10\,[kHz]$ [35]. Similarly, the MAE of $8.51\,[ms]$ for the LVET estimates compare well to previously published results. Specifically, [53] reported LVET MAEs of $29.9\,[ms]$, $14.4\,[ms]$, and $11.5\,[ms]$, when using the ICG, PCG, and PPG, respectively (17 subjects; PCG sampling rate: $44.1\,[kHz]$), while the PCG-based method presented in [54] resulted in MAEs of $11.39\,[ms]$ and $17.51\,[ms]$ for populations of 23 healthy subjects and 12 subjects suffering from different cardiovascular diseases, respectively (sampling rate: $44.1\,[kHz]$). However, as a word of caution, we note that there is some uncertainty both in the manual annotation, and in the relation between the cardiac events and the SCG waveform [55].

IV. Summary

We have developed an HMM-based method for processing SCGs. Each state in the HMM represents a stage in the cardiac cycle. After estimating the cardiac state at each sampling instance, the obtained sequence of states can be used to estimate heart rate, HRV measures, and cardiac time intervals. The proposed algorithm was evaluated on data from 67 subjects. For the estimation of heart rate and HRV measures, comparisons were made against previously proposed envelope-based and spectral-based methods. The proposed HMM-based method demonstrated a superior performance in all respects, achieving a MAE of the beat-to-beat interval in the order of $5\,[ms]$. Estimated cardiac time intervals and time points for cardiac events were benchmarked against manual annotations. The resulting MAEs were about $5\,[ms]$ for the cardiac events, and $5\,[ms]$ and $9\,[ms]$ for the IVCT and LVET intervals, respectively. Continued studies of SCGs were motivated by favorable comparisons with results reported in studies using competing sensor modalities.

[4]To assess the inter-annotation variability of the ground truth, we let an independent expert annotate the same events on data from two subjects. The mean absolute differences of the timings obtained from the two annotators were less than $0.4\,[ms]$ for all events, and hence, they were well below the typical estimation error.

TABLE V
ABSOLUTE ERRORS (MEAN ± STANDARD DEVIATION) OF ESTIMATED TIME POINTS FOR CARDIAC EVENTS AND ESTIMATED CARDIAC TIME INTERVALS.

	$t^{(E)}$				$\delta t^{(EE')}$	
	MC	IM	AO	AC	IVCT	LVET
Timing/time interval $[ms]$	5.49 ± 14.00	4.95 ± 13.91	5.24 ± 14.03	5.36 ± 9.53	5.10 ± 9.03	8.51 ± 15.98

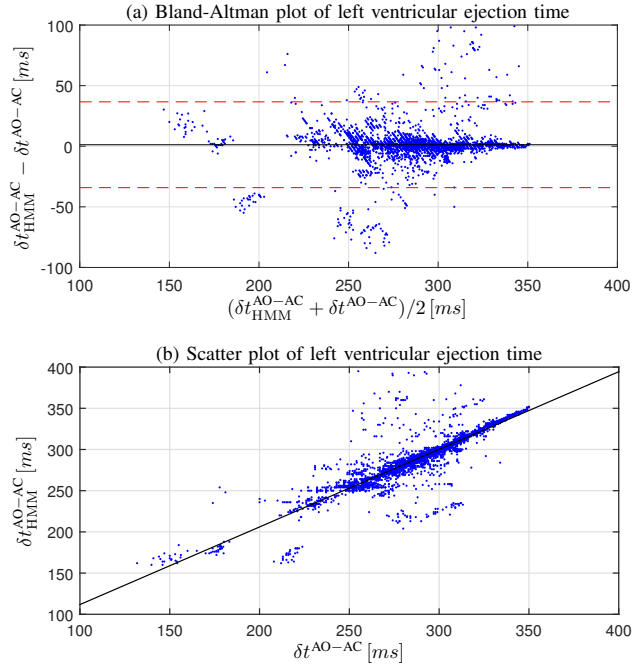

Fig. 8. Bland-Altman and scatter plot for the HMM applied to the second data set with average error (the solid black line in the Bland-Altman plot), 95 [%]-limits of agreement (the dashed red lines in the Bland-Altman plot), and fitted linear regression line (the solid black line in the scatter plot). The sample correlation coefficient of $\delta t_{\text{HMM}}^{\text{AO-AC}}$ and $\delta t^{\text{AO-AC}}$ was 0.846.

V. Possible Extensions

Most likely, there are several extensions that can be made to the presented estimation framework to increase its accuracy and extend its area of application. Here, we will briefly discuss non-exponential state duration densities, automated cardiac time interval estimation, the detection of cardiac arrhythmia, and beat-to-beat estimation of amplitudes in the SCG waveform. The use of non-exponential state duration densities, i.e., hidden semi-Markov models (HSMMs) [41], can be expected to enable a more realistic model of the time spent in state 1. HSMMs have previously been used for ECG delineation in [37] and [38]. Moreover, the state duration distributions could be adjusted to account for the temporal correlation of the beat-to-beat intervals [56].

The method for estimation of cardiac time intervals outlined in Section II-F suffers from the fact it requires new manual annotations for each considered subject. While this may be acceptable in some applications [57], [58], automated methods are more likely to achieve widespread recognition [15]. One way to resolve this issue while still utilizing the proposed HMM could be to first make manual annotations on SCG waveforms $\hat{\boldsymbol{\mu}}_n$, obtained from a restricted number of subjects, and then use machine-learning methods to obtain a general function which takes an estimated waveform as input and outputs the HMM states associated with the considered cardiac events. Moreover, it may also be possible to apply rule-based annotation methods similar to those presented in e.g., [52] and [59], to $\hat{\boldsymbol{\mu}}_n$. Either way, once the desired HMM states have been found, the time intervals can be estimated as described by (12).

Cardiac arrhythmia is a generic term for disturbances of the heart rhythm. The arrhythmias can in many instances be identified as sequences of heartbeats with unusual timing or ECG morphology. Often, features from the ECG waveform are used to classify each heartbeat into one of several arrhythmia classes [60]. Presumably, similar methods can be used to detect arrhythmias from SCGs [61], [62]. However, if each arrhythmia class gives rise to a unique SCG waveform, it may also be possible to model the occurrence of arrhythmic beats by using a hierarchical HMM (HHMM) [63]. Naturally, the top level would include one state for each arrhythmia class, and an additional resting state [38]. The substates of each state representing an arrhythmia class could then be modeled as in Section II. Similar models have previously been used in e.g., pedestrian activity classification [64].

Amplitudes and peak-to-peak amplitudes in the SCG waveform have been used to estimate cardiac output [12] and assess myocardial contractility [65]. Commonly, the estimation of amplitudes utilizes fiducial points detected from an ECG. However, since each state in the HMM presented in Section II corresponds to a specific stage in the cardiac cycle, it may be possible to estimate these amplitudes from measurements at sampling instances when the Viterbi sequence traverses a given state. For example, if the AO is determined to correspond to state $\tilde{n}$, the AO amplitude could be estimated as the average of the measurements (in the considered directions) recorded while $\hat{x}_k = \tilde{n}$ in the considered cardiac cycle. This would then eliminate the need to record a concurrent ECG.

Appendix A

This appendix describes the envelope-based heart rate estimation algorithm that was employed in Section III. Similar algorithms have previously been presented in [21], [22], and [66].

To begin with, all IMU signals are high-pass filtered using the same method as in step 1 in Algorithm 2. Following this, we compute the envelope of each IMU signal [67]. Assuming that the resulting signals are $\{\acute{\mathbf{y}}_k^a\}_{k=0}^K$ and $\{\acute{\mathbf{y}}_k^\omega\}_{k=0}^K$, the normalized energy function is computed as

$$\acute{E}_k = \frac{\|\acute{\mathbf{y}}_k^\omega\|^2}{\sum_{k_1=0}^K \|\acute{\mathbf{y}}_{k_1}^\omega\|^2} + \frac{\|\acute{\mathbf{y}}_k^a\|^2}{\sum_{k_2=0}^K \|\acute{\mathbf{y}}_{k_2}^a\|^2}. \tag{13}$$

for all k. Now, heartbeats are detected as time instances k where $\acute{E}_k = \max(\acute{E}_{k-\delta k}, \ldots, \acute{E}_{k+\delta k})$. Finally, false alarms are removed by iterating through all heartbeats from start to finish and rejecting any heartbeat occurring less than $0.5\,[s]$ after the previous heartbeat.

APPENDIX B

This appendix describes the spectral-based heart rate estimation algorithm that was employed in Section III. Similar algorithms have previously been presented in [9], [10], [23] and [24].

First, the envelope-based method is used to divide the data into segments. A segment is considered to start $0.25\,[s]$ before a heartbeat (as detected by the envelope-based method) and end $0.5\,[s]$ after the subsequent heartbeat. The data from each segment is processed independently. To start with, the accelerometer measurements (normalized to have zero mean) are high-pass filtered using a Butterworth filter of order 1 and with a cutoff frequency of $0.5\,[Hz]$. While gyroscopes also could be used, we will follow [23] and only employ accelerometers. Following this, the signals are reduced to scalar form by computing the signal which is the norm of the band-pass filtered accelerometer signals at each sampling instance. This has the advantage of creating a signal which is not dependent on the orientation in which the accelerometer was placed on the body. Last, the discrete-time Fourier transform of the signal is computed, and the heart rate is estimated as the frequency that, among the frequencies giving a local maximum of the PSD, is closest to the heart rate implied by the envelope-based method (i.e., the inverse of the estimated beat-to-beat interval of the two heartbeats).

REFERENCES

[1] "Heart disease and stroke statistics," 2015, American Heart Association.

[2] M. Malik, "Heart rate variability," *European Heart J.*, vol. 17, pp. 354–381, Mar. 1996.

[3] S. Arberet *et al.*, "Photoplethysmography-based ambulatory heartbeat monitoring embedded into a dedicated bracelet," in *Proc. Int. Conf. Comput. Cardiology*, Zaragoza, Spain, Sep. 2013, pp. 935–938.

[4] H. H. Woltjer, H. J. Bogaard, and P. M. J. M. de Vries, "The technique of impedance cardiography," *European Heart J.*, vol. 18, no. 9, pp. 1396–1403, Sep. 1997.

[5] B. S. Emmanuel, "A review of signal processing techniques for heart sound analysis in clinical diagnosis," *J. Med. Eng. Technol.*, vol. 36, no. 6, pp. 303–307, Aug. 2012.

[6] C. Bruser, S. Winter, and S. Leonhardt, "Unsupervised heart rate variability estimation from ballistocardiograms," *Int. J. Bioelectromagnetism*, vol. 15, no. 1, pp. 1–6, Jan. 2013.

[7] P.-F. Migeotte *et al.*, "Three dimensional ballistocardiogram and seismocardiogram: What do they have in common?" in *Proc. 36th IEEE Int. Conf. Eng. Med. Biol. Soc.*, Chicago, IL, Aug. 2014, pp. 6085–6088.

[8] J. Zanetti and K. Tavakolian, "Seismocardiography: Past, present and future," in *Proc. 35th IEEE Int. Conf. Eng. Med. Biol. Soc.*, Osaka, Japan, Jul. 2013, pp. 7004–7007.

[9] J. Hernandez *et al.*, "BioGlass: Physiological parameter estimation using a head-mounted wearable device," in *Proc. 4th IEEE Int. Conf. Wireless Mobile Commun. Healthcare*, Athens, Greece, Nov. 2014, pp. 55–58.

[10] J. Hernandez, D. McDuff, and R. W. Picard, "BioWatch: Estimation of heart and breathing rates from wrist motions," in *Proc. 9th IEEE Int. Conf. Pervasive Comput. Technol. Healthcare*, Istanbul, Turkey, May 2015, pp. 169–176.

[11] O. Inan *et al.*, "Ballistocardiography and seismocardiography: A review of recent advances," *IEEE J. Biomed. Health Inform.*, vol. 19, no. 4, pp. 1414–1427, Jul. 2015.

[12] P. Castiglioni *et al.*, "Wearable seismocardiography," in *Proc. 29th IEEE Int. Conf. Eng. Med. Biol. Soc.*, Lyon, France, Aug. 2007, pp. 3954–3957.

[13] M. Perlmutter and L. Robin, "High-performance, low cost inertial MEMS: A market in motion!" in *Proc. IEEE/ION Symp. Position Location and Navigation*, Myrtle Beach, SC, Apr. 2012, pp. 225–229.

[14] J. Zanetti and D. Salerno, "Seismocardiography: A technique for recording precordial acceleration," in *Proc. 4th IEEE Symp. Comput. Med. Syst.*, Baltimore, MD, May 1991, pp. 4–9.

[15] F. Khosrow-khavar *et al.*, "Automatic annotation of seismocardiogram with high-frequency precordial accelerations," *IEEE J. Biomed. Health Inform.*, vol. 19, no. 4, pp. 1428–1434, Jul. 2015.

[16] K. Tavakolian, A. Vaseghi, and B. Kaminska, "Improvement of ballistocardiogram processing by inclusion of respiration information," *Physiological Meas.*, vol. 29, no. 7, pp. 771–781, Jun. 2008.

[17] D. M. Salerno *et al.*, "Seismocardiographic changes associated with obstruction of coronary blood flow during balloon angioplasty," *American J. Cardiology*, vol. 68, no. 2, pp. 201–207, Jul. 1991.

[18] K. Tavakolian, A. Akhbardeh, and B. Kaminska, "An objective approach towards assessment of the physiological age of heart," in *Association for the Advancement of Artificial Intell.*, Washington, DC, Nov. 2008, pp. 131–133.

[19] M. Di Rienzo *et al.*, "A wearable system for the seismocardiogram assessment in daily life conditions," in *Proc. 33th IEEE. Int. Conf. Eng. Med. Biol. Soc.*, Boston, MA, Aug. 2011, pp. 4263–4266.

[20] M. J. Tadi *et al.*, "Seismocardiography: Toward heart rate variability (HRV) estimation," in *Proc. IEEE Int. Symp. Med. Meas. Appl.*, Turin, Italy, May 2015, pp. 261–266.

[21] M. Garcia-Gonzalez *et al.*, "A comparison of heartbeat detectors for the seismocardiogram," in *Proc. Int. Conf. Comput. Cardiology*, Zaragoza, Spain, Sep. 2013, pp. 461–464.

[22] D. Phan *et al.*, "Estimation of respiratory waveform and heart rate using an accelerometer," in *Proc. 30th IEEE Int. Conf. Eng. Med. Biol. Soc.*, Vancouver, BC, Aug. 2008, pp. 4916–4919.

[23] J. Hernandez, D. McDuff, and R. Picard, "BioPhone: Physiology monitoring from peripheral smartphone motions," in *Proc. 37th IEEE Int. Conf. Eng. Med. Biol. Soc.*, Milan, Italy, Aug. 2015, pp. 7180–7183.

[24] M. Haescher *et al.*, "A study on measuring heart- and respiration-rate via wrist-worn accelerometer-based seismocardiography (SCG) in comparison to commonly applied technologies," in *Proc. 2nd Int. Conf. on Sensor-based Activity Recognition and Interaction*, Rostock, Germany, Jun. 2015, pp. 2:1–2:6.

[25] C. Bruser, S. Winter, and S. Leonhardt, "Robust inter-beat interval estimation in cardiac vibration signals," *Physiological Meas.*, vol. 34, no. 2, pp. 123–138, Feb. 2013.

[26] M. Di Rienzo *et al.*, "Beat-to-beat estimation of LVET and QS2 indices of cardiac mechanics from wearable seismocardiography in ambulant subjects," in *Proc. 35th IEEE Int. Conf. Eng. Med. Biol. Soc.*, Osaka, Japan, Jul. 2013, pp. 7017–7020.

[27] M. Wolf *et al.*, "Sinus arrhythmia in acute myocardial infarction," *Med. J. Aust.*, vol. 15, no. 2, pp. 52–53, Jul. 1978.

[28] E. Vanoli *et al.*, "Heart rate variability during specific sleep stages," *Circulation*, vol. 91, no. 7, pp. 1918–1922, Apr. 1995.

[29] S. Saha *et al.*, "The potential role of short-term heart rate variability tests in identifying risk of hypertension in normotensive offspring of hypertensive parents," *Saudi J. Sports Med.*, vol. 15, no. 1, pp. 62–67, Jan. 2015.

[30] G. E. Billman, "Heart rate variability - A historical perspective," *Front. Physiol.*, vol. 2, no. 86, Nov. 2011.

[31] J. K. Oh and J. Tajik, "The return of cardiac time intervals: The phoenix is rising," *J. Am. Coll. Cardiol.*, vol. 42, no. 8, pp. 1471–1474, Oct. 2003.

[32] K. Tavakolian, "Systolic time intervals and new measurement methods," *Cardiovascular Eng. Technol.*, vol. 7, no. 2, pp. 118–125, Jun. 2016.

[33] M. J. Tadi *et al.*, "A new algorithm for segmentation of cardiac quiescent phases and cardiac time intervals using seismocardiography," in *Proc. 6th Int. Conf. Graphic Image Process.*, vol. 9443, Beijing, China, Mar. 2015.

[34] ——, "Accelerometer-based method for extracting respiratory and cardiac gating information for dual gating during nuclear medicine imaging," *Int. J. Biomed. Imag.*, Jul. 2014, ID: 690124.

[35] L. Giorgis *et al.*, "Analysis of cardiac micro-acceleration signals for the estimation of systolic and diastolic time intervals in cardiac resynchronization therapy," in *Proc. Int. Conf. Comput. Cardiology*, Bologna, Italy, Sep. 2008, pp. 393–396.

[36] F. Khosrow-khavar *et al.*, "A new seismocardiography segmentation algorithm for diastolic timed vibrations," in *Proc. 35th IEEE. Int. Conf. Eng. Med. Biol. Soc.*, Osaka, Japan, Jul. 2013, pp. 7278–7281.

[37] N. P. Hughes, N. Peter, and H. D. Philosophy, "Markov models for automated ECG interval analysis," in *Proc. NIPS 16*, Whistler, BC, Dec. 2003, pp. 611–618.

[38] D. A. Coast *et al.*, "An approach to cardiac arrhythmia analysis using hidden Markov models," *IEEE Trans. Biomed. Eng.*, vol. 37, no. 9, pp. 826–836, Sep. 1990.

[39] G. Shafiq and K. C. Veluvolua, "Surface chest motion decomposition for cardiovascular monitoring," *Scientific Reports*, vol. 4, no. 5093, 2014.

[40] L. E. Baum and T. Petrie, "Statistical inference for probabilistic functions of finite state Markov chains," *Ann. Math. Statist.*, vol. 37, no. 6, pp. 1554–1563, Dec. 1966.

[41] L. Rabiner, "A tutorial on hidden Markov models and selected applications in speech recognition," *Proc. IEEE*, vol. 77, no. 2, pp. 257–286, Feb. 1989.

[42] F. Yang, S. Balakrishnan, and M. J. Wainwright, "Statistical and computational guarantees for the Baum-Welch algorithm," in *Non-convex optimization workshop*, Montreal, QC, Dec. 2015.

[43] D. Rendon *et al.*, "Mapping the human body for vibrations using an accelerometer," in *Proc. 29th IEEE Int. Conf. Eng. Med. Biol. Soc.*, Lyon, France, Aug. 2007, pp. 1671–1674.

[44] I. Skog *et al.*, "Inertial sensor arrays, maximum likelihood, and Cramér-Rao bound," *IEEE Trans. Signal Process.*, vol. 64, no. 16, pp. 4218–4227, Aug. 2016.

[45] J. Pan and W. J. Tompkins, "A real-time QRS detection algorithm," *IEEE Trans. Biomed. Eng.*, vol. 32, no. 3, pp. 230–236, Mar. 1985.

[46] D. Giavarina, "Understanding Bland Altman analysis," *Biochem. Med .*, vol. 25, no. 2, pp. 141–151, Jun. 2015.

[47] F. Landreani *et al.*, "Beat-to-beat heart rate detection by smartphone's accelerometers: Validation with ECG," in *Proc. 38th IEEE Int. Conf. Eng. Med. Biol. Soc.*, Orlando, FL, Aug. 2016, pp. 525–528.

[48] C. Bruser *et al.*, "Multi-channel optical sensor-array for measuring ballistocardiograms and respiratory activity in bed," in *Proc. 34th IEEE Int. Conf. Eng. Med. Biol. Soc.*, San Diego, CA, Aug. 2012, pp. 5042–5045.

[49] ——, "Applying machine learning to detect individual heart beats in ballistocardiograms," in *Proc. 32th IEEE Int. Conf. Eng. Med. Biol. Soc.*, Buenos Aires, Brazil, Aug. 2010, pp. 1926–1929.

[50] J. Parak *et al.*, "Evaluation of the beat-to-beat detection accuracy of PulseOn wearable optical heart rate monitor," in *Proc. 37th IEEE Int. Conf. Eng. Med. Biol. Soc.*, Milan, Italy, Aug. 2015, pp. 8099–8102.

[51] G. D. Clifford, "Signal processing methods for heart rate variability," Ph.D. dissertation, University of Oxford, 2002.

[52] F. Khosrow-khavar, K. Tavakolian, and C. Menon, "Moving toward automatic and standalone delineation of seismocardiogram signal," in *Proc. 37th IEEE Int. Conf. Eng. Med. Biol. Soc.*, Milan, Italy, Aug. 2015, pp. 7163–7166.

[53] P. Carvalho *et al.*, "Comparison of systolic time interval measurement modalities for portable devices," in *Proc. 32th IEEE Int. Conf. Eng. Med. Biol. Soc.*, Buenos Aires, Argentina, Aug. 2010, pp. 606–609.

[54] R. P. Paiva *et al.*, "Beat-to-beat systolic time-interval measurement from heart sounds and ECG," *Physiol. Meas.*, vol. 33, no. 2, pp. 177–194, Feb. 2012.

[55] J. M. Zanetti, M. O. Poliac, and R. S. Crow, "Seismocardiography: Waveform identification and noise analysis," in *Proc. IEEE Int. Conf. Comput. Cardiology*, Venice, Italy, Sep. 1991, pp. 49–52.

[56] F. Lee and A. Nehorai, "Adaptive power spectrum estimation algorithm for heart rate variability analysis," in *Proc. Int. Conf. Comput. Cardiology*, Venice, Italy, Sep. 1991, pp. 273–276.

[57] A. K. Ka, "ECG beats classification using waveform similarity and RR interval," *CoRR*, vol. arXiv:1101.1836, Jan. 2011.

[58] B. Frenay, G. de Lannoy, and M. Verleysen., "Emission modelling for supervised ECG segmentation using finite differences," in *Proc. 4th European Int. Conf. Int. Federation for Med. and Biomed. Eng.*, Anvers, Belgium, Nov. 2008, pp. 1212–1216.

[59] A. Laurin *et al.*, "Accurate and consistent automatic seismocardiogram annotation without concurrent ECG," in *Proc. Int. Conf. Comput. Cardiology*, Nice, France, Sep. 2015, pp. 25–28.

[60] P. de Chazal, M. O'Dwyer, and R. B. Reilly, "Automatic classification of heartbeats using ECG morphology and heartbeat interval features," *IEEE Trans. Biomed. Eng.*, vol. 51, no. 7, pp. 1196–1206, Jul. 2004.

[61] C. I. Stefanadis, "Bioelectronics: The way to discover the world of arrhythmias?" *Hellenic J. Cardiology*, vol. 55, pp. 267–268, May 2014.

[62] R. Uhashini, S. Dhanalakshmi, and R. Vasanthi, "A survey on the scope of cardiac arrhythmia classification using BCG," *Int. J. Innovative Research Technol. Sci.*, vol. 2, no. 6, pp. 41–46, Nov. 2014.

[63] S. Fine, Y. Singer, and N. Tishby, "The hierarchical hidden Markov model: Analysis and applications," *Mach. Learn.*, vol. 32, no. 1, pp. 41–62, Jul. 1998.

[64] G. Panahandeh *et al.*, "Continuous hidden Markov model for pedestrian activity classification and gait analysis," *IEEE Trans. Instrum. Meas.*, vol. 62, no. 5, pp. 1073–1083, May 2013.

[65] K. Tavakolian *et al.*, "Myocardial contractility: A seismocardiography approach," in *Proc. 34th IEEE Int. Conf. Eng. Med. Biol. Soc.*, San Diego, CA, Aug. 2012, pp. 3801–3804.

[66] J. Ramos-Castro *et al.*, "Heart rate variability analysis using a seismocardiogram signal," in *Proc. 34th IEEE Int. Conf. Eng. Med. Biol. Soc.*, San Diego, CA, Aug. 2012, pp. 5642–5645.

[67] J. Dugundji, "Envelopes and pre-envelopes of real waveforms," *IRE Trans. Inf. Theory*, vol. 4, no. 1, pp. 53–57, Mar. 1958.

Johan Wahlström received his MSc degree in Engineering Physics from the KTH Royal Institute of Technology, Stockholm, Sweden, in 2014. He subsequently joined the Signal Processing Department at KTH, working towards his PhD. His main research topic is insurance telematics. In 2015, he received a scholarship from the Sweden-America foundation and spent six months at Washington University, St. Louis, USA.

Isaac Skog (S'09-M'10) received the BSc and MSc degrees in Electrical Engineering from the KTH Royal Institute of Technology, Stockholm, Sweden, in 2003 and 2005, respectively. In 2010, he received the PhD degree in Signal Processing with a thesis on low-cost navigation systems. In 2009, he spent 5 months at the Mobile Multi-Sensor System research team, University of Calgary, Canada, as a visiting scholar and in 2011 he spent 4 months at the Indian Institute of Science (IISc), Bangalore, India, as a visiting scholar. He is currently a Researcher at KTH coordinating the KTH Insurance Telematics Lab. He was a recipient of a Best Survey Paper Award by the IEEE Intelligent Transportation Systems Society in 2013.

Peter Händel (S'88-M'94-SM'98) received a PhD degree from Uppsala University, Uppsala, Sweden, in 1993. From 1987 to 1993, he was with Uppsala University. From 1993 to 1997, he was with Ericsson AB, Kista, Sweden. From 1996 to 1997, he was a Visiting Scholar with the Tampere University of Technology, Tampere, Finland. Since 1997, he has been with the KTH Royal Institute of Technology, Stockholm, Sweden, where he is currently a Professor of Signal Processing and the Head of the Department of Signal Processing. From 2000 to 2006, he held an adjunct position at the Swedish Defence Research Agency. He has been a Guest Professor at the Indian Institute of Science (IISc), Bangalore, India, and at the University of Gävle, Sweden. He is a co-founder of Movelo AB. Dr. Händel has served as an associate editor for the *IEEE Transactions on Signal Processing*. He was a recipient of a Best Survey Paper Award by the IEEE Intelligent Transportation Systems Society in 2013.

Farzad Khosrow-khavar received the B.Eng. degree in electrical engineering and the MSc degree in computer engineering from the University of Victoria, Victoria, BC, Canada. Since 2010, he has worked as a PhD candidate in the MENRVA lab at Simon Fraser University, Burnaby, BC, Canada. He works in the area of biomedical signal processing and cardiovascular vibration modeling.

Kouhyar Tavakolian received the PhD degree from Simon Fraser University, Burnaby, BC, Canada, in 2010. Currently, he is a Postdoctorate Fellow in the Electrical and Computer Engineering Department of the University of British Columbia, Vancouver, BC, Canada. His area of research is the processing of bio-signals such as EEG, ECG, and different types of mechanocardiograms.

Phyllis K. Stein received her AB in Physics from Barnard College, New York, in 1959, and her M.Ed. in Exercise Physiology and PhD in Health Promotion from University of Virginia, Charlottesville, in 1987 and 1990, respectively. Dr. Stein is an Associate Professor of Medicine at the Division of Cardiology, Washington University School of Medicine, where she also is the Director of the Heart Rate Variability (HRV) Laboratory. Her current research interest includes the integration of heart-rate-based markers, including HRV, and information from polysomnography as markers of cardiovascular autonomic and central nervous system function, and as predictors of functional status and survival in the elderly.

Arye Nehorai (S'80-M'83-SM'90-F'94) is the Eugene and Martha Lohman Professor of Electrical Engineering in the Preston M. Green Department of Electrical and Systems Engineering (ESE) at Washington University in St. Louis (WUSTL). He served as chair of this department from 2006 to 2016. Under his department chair leadership, the undergraduate enrollment has more than tripled in four years and the master's enrollment grew seven-fold in the same time period. He is also Professor in the Department of Biomedical Engineering (by courtesy), Professor in the Division of Biology and Biomedical Studies (DBBS), and Director of the Center for Sensor Signal and Information Processing at WUSTL. Prior to serving at WUSTL, he was a faculty member at Yale University and the University of Illinois at Chicago. He received the BSc and MSc degrees from the Technion, Israel and the PhD from Stanford University, California.

Dr. Nehorai served as Editor-in-Chief of the *IEEE Transactions on Signal Processing* from 2000 to 2002. From 2003 to 2005 he was the Vice President (Publications) of the IEEE Signal Processing Society (SPS), the Chair of the Publications Board, and a member of the Executive Committee of this Society. He was the founding editor of the special columns on Leadership Reflections in *IEEE Signal Processing Magazine* from 2003 to 2006.

Dr. Nehorai received the 2006 IEEE SPS Technical Achievement Award and the 2010 IEEE SPS Meritorious Service Award. He was elected Distinguished Lecturer of the IEEE SPS for a term lasting from 2004 to 2005. He received several best paper awards in IEEE journals and conferences. In 2001 he was named University Scholar of the University of Illinois. Dr. Nehorai was the Principal Investigator of the Multidisciplinary University Research Initiative (MURI) project titled Adaptive Waveform Diversity for Full Spectral Dominance from 2005 to 2010. He is a Fellow of the IEEE since 1994, Fellow of the Royal Statistical Society since 1996, and Fellow of AAAS since 2012.